scientific reports

Check for updates

OPEN

Numerical study on a facing electrode configuration dielectrophoresis microfluidic system for efficient biological cell separation

Thu Hang Nguyen[1], Hoang Trung Nguyen[1], Nam Anh Ngo[1], Mai Chi Nguyen[1], Hang Bui Thu[1,2], Jens Ducrée[3], Trinh Chu Duc[1], Thanh Tung Bui[1] & Loc Do Quang[4]✉

Circulating tumor cell separation has been the focus of numerous studies owing to its importance in the diagnosis, prognosis, and therapy of cancer. This study reports a highly efficient microfluidic device that integrates a specialized dielectrophoresis configuration, namely the facing-electrode configuration dielectrophoresis (FEC-DEP) structure, to isolate circulating tumor cells (CTCs) from various blood components, including red blood cells, white blood cells, and platelets. The FEC-DEP design features a bottom-slanted electrode array positioned parallel to a basic rectangular top electrode. A non-homogeneous electric field is produced between these parallel electrodes, generating dielectrophoretic forces acting on cells. Consequently, when the FEC-DEP is integrated into a flow, it can direct various biological objects in the flow along separate trajectories. As a result, cells with comparable characteristics might move together within a similar path. This configuration may simplify the microfabrication process and lessen dependency on particle position within the microchannel. The separation process was numerically analyzed using the finite element method, and device parameters were optimized to obtain high-efficiency and high-purity cell separation. The simulations show that the microfluidic device may effectively enrich tumor cells in a label-free and non-invasive manner, with a high-efficiency rate of almost 80%.

Keywords Dielectrophoresis, Microfluidic chip, Cell separation, Cancer cell analysis

Many biochemical and biomedical applications necessitate cellular manipulations and separations to facilitate the identification, isolation, and investigation of phenotypes or samples of interest. For example, the process of isolating blood cells in a sample is crucial due to the distinct functions that each blood component serves, especially in the case of cancer patients[1,2]. During the pre-metastatic stage, the presence of cancer cells in the bloodstream and lymphatic system offers valuable clinical information for diagnosing the medical condition and determining appropriate treatment plans for patients[3–5]. In regenerative medicine, the separation and purification of stem cells play an important role to study the heterogeneity of stem cell populations and assure the safety and efficiency of treatment[6,7]. In reproductive biology and assisted reproductive technologies, the first steps to better treatments for infertility are to separate, and select high-quality reproductive cells in a lab setting. These cells include motile sperm and highly competent oocytes[8,9]. In addition, the aim of prenatal diagnosis has shifted to non-invasive methods using fetal cells circulating in maternal peripheral blood in order to collect entire fetal genetic information while minimizing dangers to the mother and fetus[10]. The creation of separation methods with great efficiency is required to extract the rare fetal cells from the mother's blood[10]. Thanks to the ability to precisely control fluids in micro-scale channels, microfluidic platforms have been widely used for cell manipulation and separation in blood samples. Microfluidic cell separation is a cutting-edge technology with numerous applications in both research and clinical settings such as rare cell separation from blood sample[11], stem cell sorting and isolation[7], reproductive cell manipulation, sorting and separation[12,13], etc. These platforms

[1]University of Engineering and Technology, Vietnam National University, Hanoi, Vietnam. [2]Faculty of Mathematics and Computer Science, Babes-Bolyai University, Cluj-Napoca, Romania. [3]School of Physical Sciences, Dublin City University, Dublin, Ireland. [4]University of Science, Vietnam National University, Hanoi, Vietnam. ✉email: locdq@vnu.edu.vn

provide many benefits, such as reduced sample volume, enhanced patient safety, and expedited analysis[14]. Microfluidics-based label-free approaches for cell isolation are primarily categorized into passive, active, and hybrid techniques based on differences in cell properties. Active approaches such as dielectrophoresis, magnetophoresis, acoustophoresis, etc. employ additional forces in the microfluidic chips[15–20]. Although enhancing the separation efficacy by adding another control level of cell trajectories, active approaches may lead to cell damage and equipment requirements[21]. In contrast, passive technologies utilize hydrodynamic force and chip geometry to distinguish cancer cells from other cell types. This approach, which does not need any additional equipment, presents a more simplified operating procedure. Nevertheless, it often experiences an extended period of analysis[21].

Dielectrophoresis (DEP) is a modern, non-invasive technology used for determining the electrical properties of biological objects, enabling further analysis and manipulation of target cells within the sample[22,23]. DEP is a method that involves the application of a force on a particle that is neutral but polarized when it encounters a non-homogeneous electric field[24,25]. DEP have been proven to effectively manipulate and separate various biological cells including cancer cells[26], stem cells[27], blood cells[15], motile sperms[28], dead and viable cells[29], etc. In the field of oncology research, the detection and separation of CTCs from various blood constituents, including white blood cells, red blood cells, platelets, and plasma, pose significant challenges due to the extremely low number of CTCs present in the blood sample and the biophysical heterogeneity among the CTC population[30]. Varmazyari et al. proposed a DEP-based microfluidic system, that used parallel sidewall electrodes. This system had encouraging outcomes, achieving a separation efficiency of 90% for CTCs[31]. However, the fabrication process is complex for setting up electrodes at the sidewall.

Additionally, several research groups have proposed microfluidic chips with embedded electrodes on only a single side of the microchannel in order to facilitate cell separation[32,33]. A recent paper designed and simulated a microfluidic chip that contained coplanar electrodes to separate CTCs (MDA-MB-231 cell line) and RBCs and obtained an efficiency of more than 90% under optimal conditions[32]. In another study, Wu et al. introduced a biochip including coplanar electrodes positioned only at the bottom of the microchannel to trap yeast cells and polystyrene microbeads suspended in diverse aqueous solutions, each exhibiting a specific conductivity[33]. Results were promising, with a single yeast cell occupancy of over 72% achievable. Nevertheless, this technique necessitates a significant concentration of the electric field around the electrode area, thus compromising resolution due to the positional dependence of the DEP force.

Recently, numerous research investigations utilized a microfluidic chip to separate different cell lines based on DEP and the findings demonstrated good matches between numerical and experimental results[34–36]. As an example, recent work suggested the use of a zigzag shape microfluidic channel to accomplish the separation of platelets by DEP forces generated by a non-uniform electric field that influenced cell movement[34]. The authors used COMSOL Multiphysics software to optimize the device design and operating settings, simulate cell trajectories under various conditions, and investigate the effects of significant factors on separation efficiency. At a voltage of 20 V and a velocity ratio of 1:4, the microfluidic chip that was fabricated with the ideal structure demonstrated a separation efficiency of 99.4%.

Our work aims to apply DEP methods to isolate CTCs from cancer patients' blood cells. The proposed microfluidic system is illustrated in Fig. 1. The proposed microfluidic system consists of two inlets and four outlets, and an integrated DEP structure, namely the facing-electrode configuration dielectrophoresis (FEC-DEP) structure. The FEC-DEP structure comprises a bottom-slanted electrode array positioned parallel to a basic rectangular top electrode. These facing electrodes with FEC-DEP design generate a non-uniform electric field causing DEP forces.

In our previous study, a microfluidic device was introduced to enrich CTCs from a mixture of red blood cells (RBCs) and white blood cells (WBCs) featuring three distinct output configurations[37]. In the current study, we have further optimized this system to efficiently separate CTCs from all major cell types found in processed blood samples, including RBCs, WBCs, and platelets (PLTs). In this study, HT-29 is used to represent CTCs in blood stream. HT-29 is a type of human colon adenocarcinoma cell line commonly utilized in biomedical research, especially for studies into cancer biology, drug development, and cancer therapy[38]. Prior to introduction into the microfluidic chip, blood samples undergo preprocessing steps to retain four types of cells including CTCs, WBCs, RBCs, and PLTs, and are then diluted in phosphate-buffered saline (PBS) to achieve an appropriate concentration. Following this preparation, a stream of blood cells – comprising RBCs, WBCs, and PLTs – is directed into the chip's inlets. Once inside, the cells encounter a non-uniform electric field, due to the distinguishable electrical properties and sizes of blood cells and tumor cells, which subjects them to different DEP forces. The differential application of force causes the cell types to follow distinct trajectories inside the microchannel and concentrate at different exits of the channel.

The proposed microfluidic device is expected to provide a potentially effective, small-scale, simply integrated, and affordable solution for CTC separating.

Theoretical analysis

In microfluidic systems, laminar flow occurs when the Reynolds number (Re) is low, typically less than one, indicating that inertial forces are negligible compared to viscous forces. The fluid flow behavior is described by the Navier-Stokes, viscous forces dominate, and inertial forces can be disregarded. Torsional flow, also known as Stokes flow, is prevalent in systems with high viscosity or small geometric length scales. Fluids in microfluidic systems can be either compressible or incompressible, and exhibit Newtonian or non-Newtonian behavior. In the analysis of such flows, momentum balance and mass conservation equations are simplified due to the dominance of viscous forces, characteristic of Stokes flow[39]:

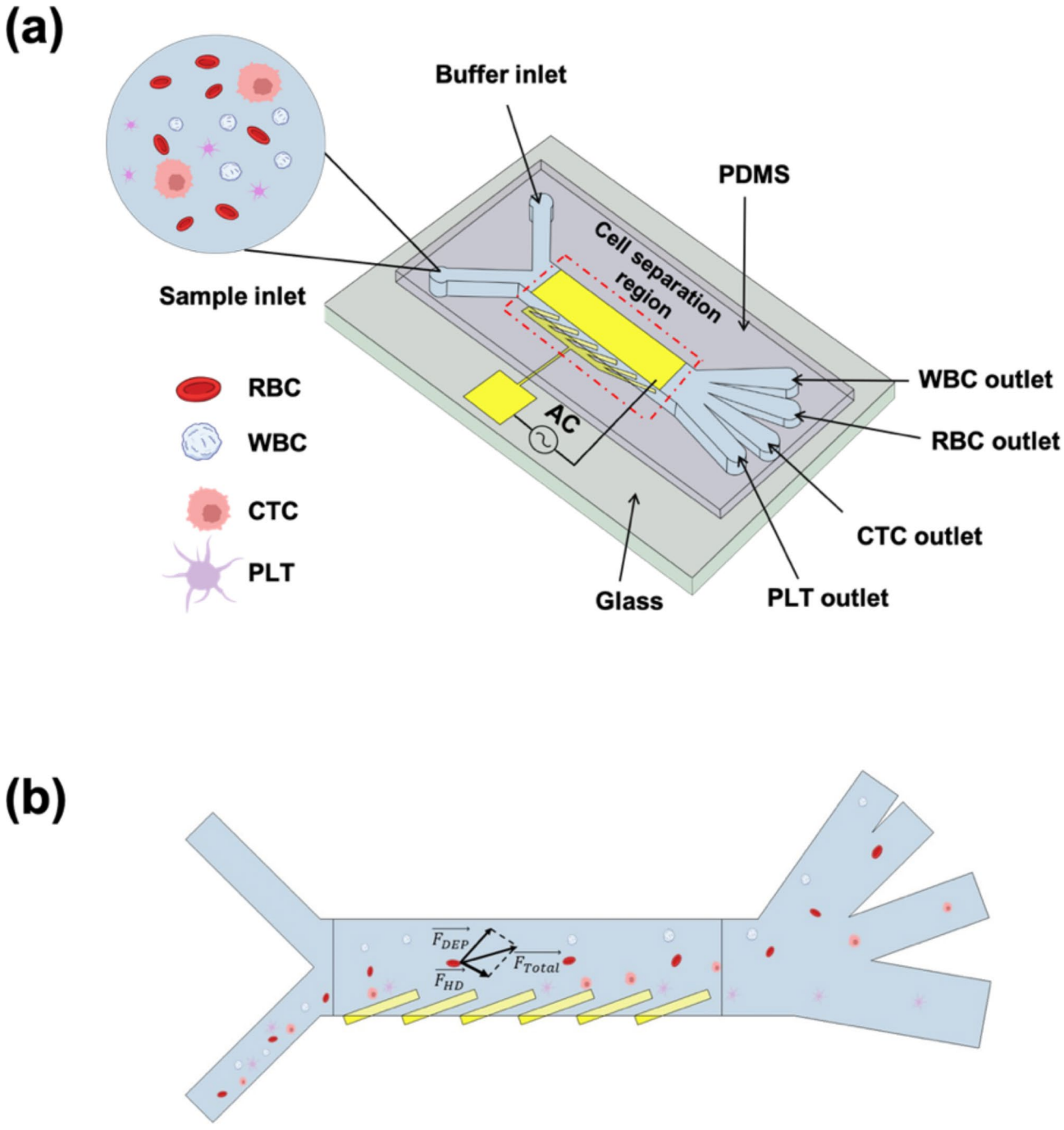

Fig. 1. (**a**) Design of the proposed microfluidic chip with integrated facing-electrode configuration dielectrophoresis (FEC-DEP) structure for separating CTCs from blood constituents, (**b**) concept of the FEC-DEP-based device: top-view.

$$\nabla \cdot \left[-p\overrightarrow{I} + \overrightarrow{K}\right] + \overrightarrow{F} = 0 \tag{1}$$

$$\frac{\delta \rho}{\delta t} + \nabla \cdot (\rho \overrightarrow{v_m}) = 0 \tag{2}$$

Here, p is the pressure, $\overrightarrow{K}$ is the viscous stress tensor, $\overrightarrow{F}$ is the volume force vector, ρ is the fluid density, and $\overrightarrow{v_m}$ is the fluid velocity.

Hydrodynamic force on a (single) suspended (rigid) particle is governed by Stokes' law in a microfluidic channel:

$$\overrightarrow{F_{HD}} = 6\pi\ \eta\ R_p(\overrightarrow{v_m} - \overrightarrow{v_p}) \tag{3}$$

Here, R_p is the radius of the bioparticle, η is the dynamic viscosity coefficient of the medium and $\overrightarrow{v_m}$is the velocity of the flow.

The electric field distributed within the proposed FEC-DEP device is governed by the current conservation based on Ohm's law[40]:

$$\nabla . \overrightarrow{J} = Q_{j,v} - \overrightarrow{J} = \sigma\ \overrightarrow{E} + \overrightarrow{J_e} \tag{4}$$

in which $\overrightarrow{J}$ denotes current density, $Q_{j,v}$ is the volumetric source of current, σ represents electrical conductivity, and $\overrightarrow{J_e}$ is an externally generated current density.

The electric potential V is calculated by the relationship with the electric field $\overrightarrow{E}$:

$$\overrightarrow{E} = -\nabla V \tag{5}$$

The motion of particles induced by DEP commences when a non-uniform electric field is applied, creating a polarization gradient between the cells and the surrounding medium. DEP mechanism relies on the size and electrical properties of particles, as well as the binding characteristics of proteins and particle surfaces, to produce specific particle deflection[41]. When particles encounter this non-homogeneous electric field, two distinct forces are exerted between them and the surrounding medium, resulting in a net force. The direction of particle movement can be influenced by either positive DEP (p-DEP) or negative DEP (n-DEP) effects, determined by the relative polarizability of the particle and the suspension medium. p-DEP happens as particles migrate towards regions of high electric field gradients, whereas n-DEP occurs when particles move towards areas of decreasing electric field gradients. Both effects are influenced by the Clausius-Mossotti relation. The DEP force driving the particle is calculated by the equation[42]:

$$F_{DEP} = 2\pi\ {R_p}^3 \varepsilon_f \mathrm{Re}\left(K_{CM}\right) \nabla \left|\overrightarrow{E}\right|^2 \tag{6}$$

where R_p is the cell radius, ε_{f} is the permittivity of the medium. K_{CM} or Clausius-Mossotti (CM) factor of particle is expressed by this equation:

$$K_{CM} = \frac{\varepsilon_c^* - \varepsilon_f^*}{\varepsilon_c^* + 2\varepsilon_f^*} \tag{7}$$

The complex permittivity ε^* of both particle (or cells in this study (c)) and the fluid (f) are calculated as follows:

$$\varepsilon^* = \varepsilon - j\frac{\sigma}{\omega} \tag{8}$$

The polarizability of the particles is measured by the real part of CM factor which is determined by permittivity ε and the electrical conductivity σ; ω = 2πf is the angular frequency of driving AC voltage, and j is the imaginary part defined as $j^2 = -1$. The Re{CM} can be adjusted within the range of -0.5 to 1 by altering the frequency of the voltage, leading to negative DEP (n-DEP) or positive DEP (p-DEP). At the crossover frequency, the term Re{CM} vanishes. The magnitude of the $(\nabla\left|\overrightarrow{E}\right|^2)$ is another important factor influencing the interaction with a particle which is dependent on the driving voltage. From Eq. 5, the gradient of electric field magnitude $\left|\overrightarrow{E}\right|^2$ depends on the gradient of the squared gradient of the potential (voltage) changes over space. The design of the fluidic chip-integrated electrode is required to increase $\nabla\left|\overrightarrow{E}\right|^2$, and to regulate other electrokinetic forces[43].

The corresponding relative complex dielectric constant of a cell, encompassing the cell membrane and interior, is substituted for the complex dielectric constant of the particle when calculating the DEP force (Fig. 2). The single-shell model describes the complicated permittivity of the cell$\varepsilon_c{}^*$ as follows[44]:

$${\varepsilon_c}^* = {\varepsilon_{mem}}^* \frac{\left(\frac{R}{R-d_{mem}}\right)^3 + 2\frac{{\varepsilon_{cyt}}^* - {\varepsilon_{mem}}^*}{{\varepsilon_{cyt}}^* + 2{\varepsilon_{mem}}^*}}{\left(\frac{R}{R-d_{mem}}\right)^3 - \frac{{\varepsilon_{cyt}}^* - {\varepsilon_{mem}}^*}{{\varepsilon_{cyt}}^* + 2{\varepsilon_{mem}}^*}} \tag{9}$$

Biological cells in the microchannel undergo the DEP force as they follow the streamlines of fluid flow. The DEP force ($\overrightarrow{F_{DEP}}$), which is directed perpendicular to the flow, and the hydrodynamic force ($\overrightarrow{F_{HD}}$) are the primary factors influencing cell movement. Minor affected forces such as gravity and Brownian motion are generally ignored as the cell radius is greater than 1 μm as indicated in Table 1. Newton's second law, which accounts for the combined vector forces of DEP and hydrodynamics, determines the velocity and trajectory of the cell:

$$\overrightarrow{F_{HD}} + \overrightarrow{F_{DEP}} = m_p \frac{d\overrightarrow{v_p}}{dt} \tag{10}$$

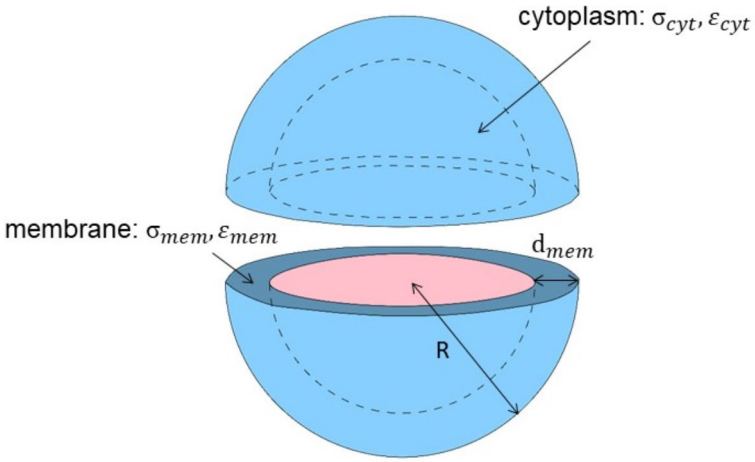

Fig. 2. Single-shell cell model.

Parameter	HT-29	RBC	WBC	PLT
Density (g/l)	1077	1110	1080	1064.5
Diameter (μm)	11	6	14	2.5
Relative permittivity	120	59	150	50
Electrical conductivity (S/m)	0.72	1.31	0.76	0.25
Shell thickness (nm)	4	8	7	7
Shell relative permittivity	11.1	4.44	6.01	6
Shell electrical conductivity (S/m)	34×10^{-6}	1×10^{-6}	24×10^{-6}	1×10^{-6}

Table 1. Electrical properties of each cell type[15,45–47].

where $\overrightarrow{v_p}$ represents the velocity and m_p stands for the mass of the cell, respectively.

Design of microfluidic device and simulation model

To produce the DEP effect and separate CTCs from blood cells, FEC-DEP has been used with a parallel electrode on top of a microfluidic system and a slanted electrode array embedded in the bottom (Fig. 3). The blood sample containing PLTs, RBCs, WBCs, and HT-29 tumor cells, as well as the buffer solution, are injected through two inlets on the biochip platform. The FEC-DEP design is placed in the center of the microchannel as the separation region, and four different outlets are positioned at the end to collect four types of cells. The ground electrode at the top of the microchannel is set as ground while and herringbone-patterned electrode array at the bottom is configured as positive polarity. The geometrical parameters of the chip are shown in Fig. 3. The electrode length of 80 μm was determined based on a combination of factors including manufacturability, the scale of the biological samples, and electrical field requirements for effective dielectrophoretic manipulation. The inlets are tilted at angles of 45° and the outlets are inclined at angles of 35°, 45°, 70° and 110° to the horizontal axis for the WBC, RBC, HT-29, and PLT outlets, respectively. The tilted angles and geometrical parameters of outlets are optimized based on the trajectories of each cell type. The biochip parameters could be further adjusted for other biological object separations with different sizes and electrical characteristics.

At the beginning of the separation process, the diluted blood sample which includes RBCs, WBCs, PLTs, and CTCs, is injected into the inlet channel at a flow rate of 200 μm/s, while the buffer solution flows at 900 μm/s. The suspending medium is phosphate-buffered saline (PBS), which has a conductivity of 55 mS/m and a relative permittivity of 80[45]. Owing to differences in size and electrical characteristics between various cell types, different DEP effects are delivered to WBCs, RBCs, PLTs, and HT-29 cells, guiding each type of cell along a particular trajectory. Interestingly, the DEP effects on cells along the y-axis intensify as the electrode angle increases. This technique makes it possible to separate CTCs from other blood cells efficiently, providing a potential platform for cancer research.

An inhomogeneous electric field induces dielectrophoresis (DEP) force in all particles, causing them to migrate away from the electrode region and upward. In this biochip, because of the impacts of the buffer flow, HT-29 cells and PLTs tend to deflect toward the sidewall close to the electrodes. Equation 6 illustrates that the strength of the DEP force is proportional to the third-order cell size. As a result, WBCs are subjected to the highest DEP force and forced to outlet 1. In contrast, PLTs undergo the least amount of DEP force and are

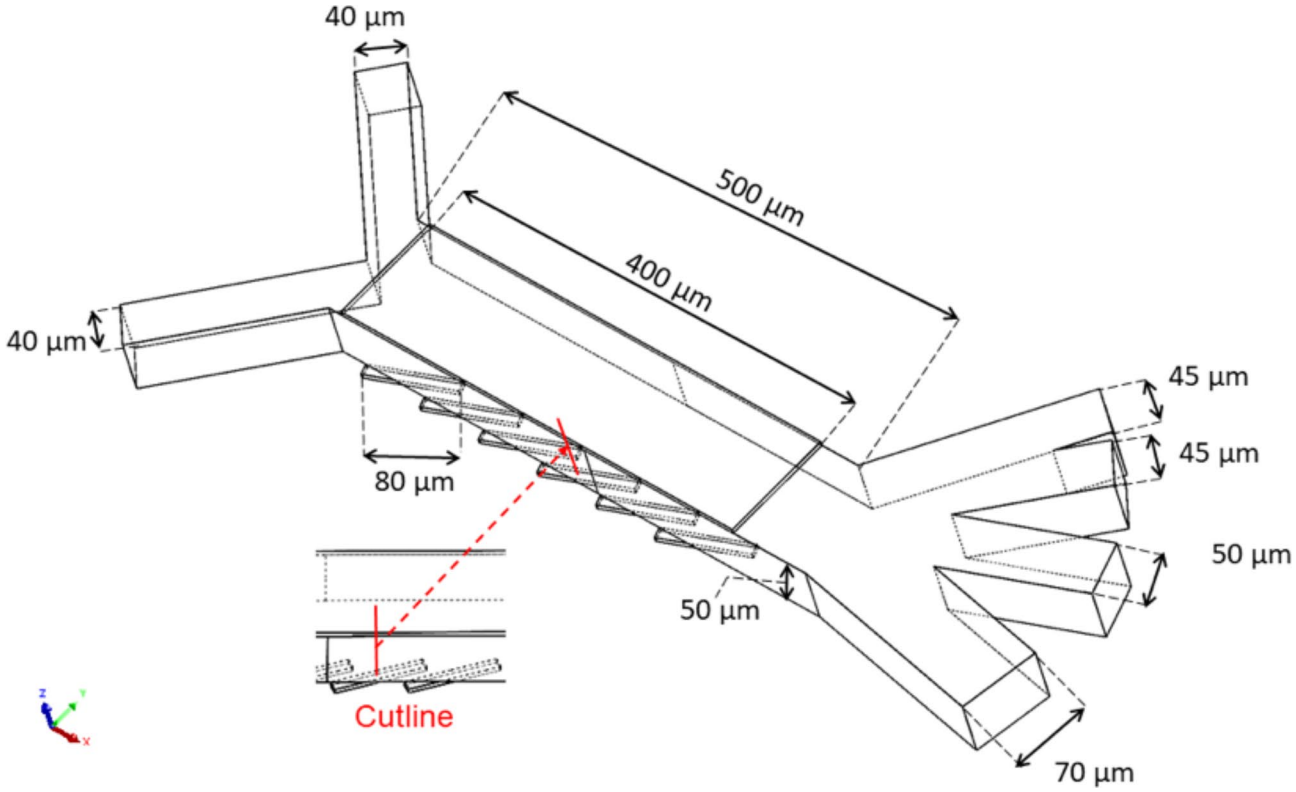

Fig. 3. Illustration of the proposed microfluidic system with dimensions of fluidic channel and FEC-DEP structure.

Mesh type	Maximum element size (µm)	Minimum element size (µm)	Maximum element growth rate	Curvature factor	Number of domain elements	Number of boundary elements
Extra fine	45.6	3.32	1.4	0.4	521,536	50,379
Finer	66.4	8.29	1.45	0.5	207,121	25,241
Fine	82.9	14.9	1.5	0.6	93,356	14,238
Normal	124	23.2	1.6	0.7	31,891	7060
Coarse	158	33.2	1.7	0.8	15,905	4438

Table 2. Mesh independency test: mesh element quality and size of four mesh types.

collected at outlet 4, since they have the smallest diameter. RBCs and HT-29 cells are collected at outlets 2 and 3, respectively. The ratio of blood sample to buffer flow rate is 1:4.5, while the applied voltage is 6 V and the AC voltage frequency is 1 kHz.

Table 1 provides the electrical characteristics of single-shell cells used in simulations[15,45–47]. WBCs comprise different subtypes such as granulocytes, monocytes, and lymphocytes, each exhibiting distinct characteristics, including size. In this work, to reduce computational complexity for the simulation process, representative parameters for WBCs that have been employed in other related studies within the field are used[45,46,48].

COMSOL Multiphysics software has been used to examine the separation mechanism, the efficiency of the microfluidic device, and the impacts of various factors on the cell separation process using a 3D model. To model and simulate this biochip, the Electric Currents, Creeping Flow, and Particle Tracing for Fluid Flow modules were utilized. The Creeping Flow accounts for the fluid behavior and velocity profile across the channel following the Stokes equation and continuity equation. To calculate the frequency-dependent electric field, the Electric Currents solve for Ohm's law. Finally, the Particle tracing module permits the evaluation of DEP forces exerting on cells, and particle trajectories under total forces. The "no-slip" and "freeze" conditions on the channel walls ensured that there was very little fluid velocity close to the walls and that the location and velocity of the particles were maintained when they collided with the wall. All cells were added to the sample inlet at random. The mesh was meticulously defined with fine-resolution mesh at the electrode regions. The mesh independent test was conducted using four mesh types: extra fine, finer, fine, normal, and coarse with different element sizes and numbers of domain and boundary elements. The mesh qualities are summarized in Table 2. The velocity field and the electric potential distribution in the microchannel have a direct influence on the separation process

and efficiency. Therefore, the mesh independence study was carried out by computing the velocity and electric potential along the cut line near the electrode as shown in Fig. 4.

Considering the computational complexity, resources, and accuracy of the simulation, in this work, the fine mesh was selected. The meshing model and the boundary conditions are shown in Fig. 5.

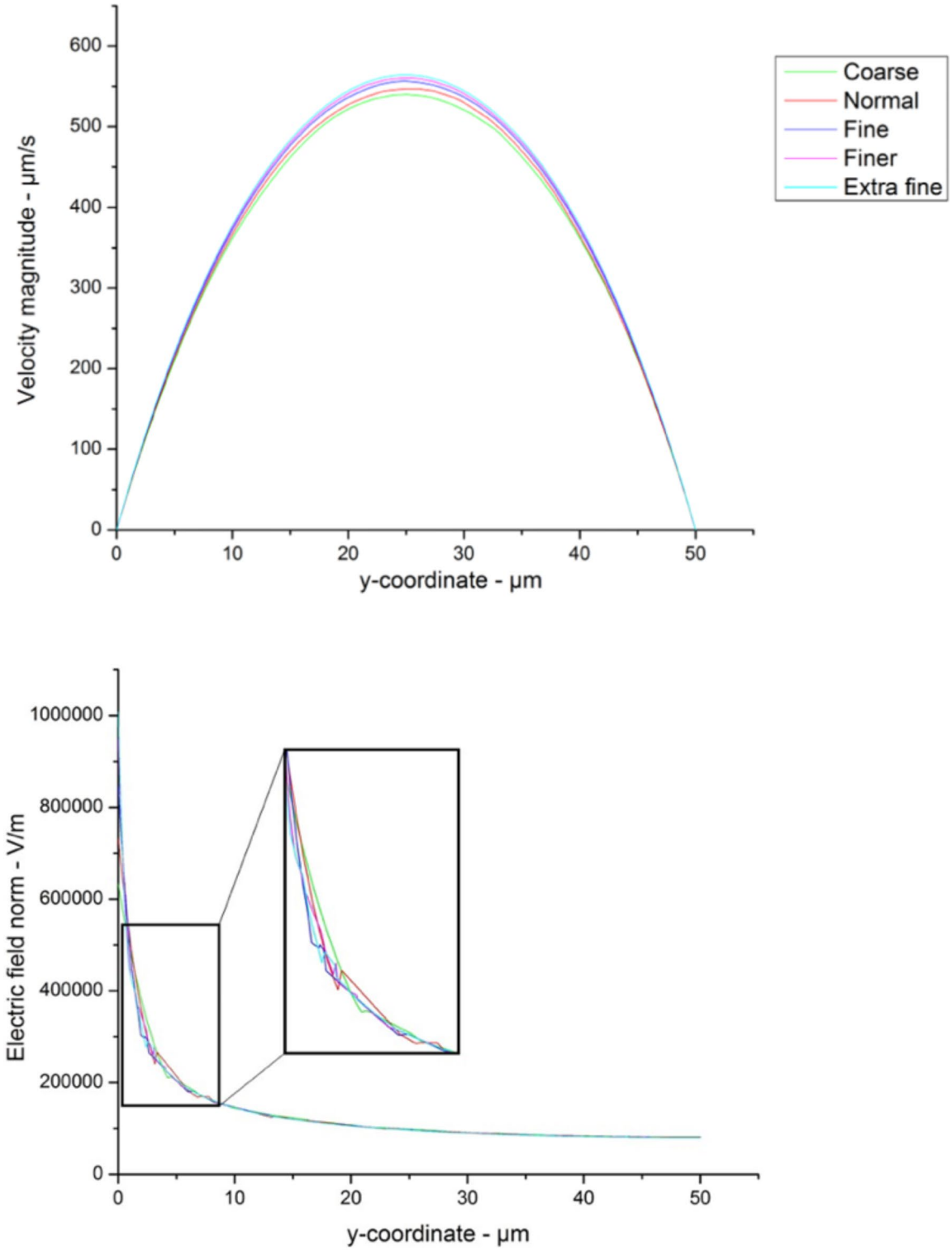

Fig. 4. Velocity magnitude and electric field norm across the cutline.

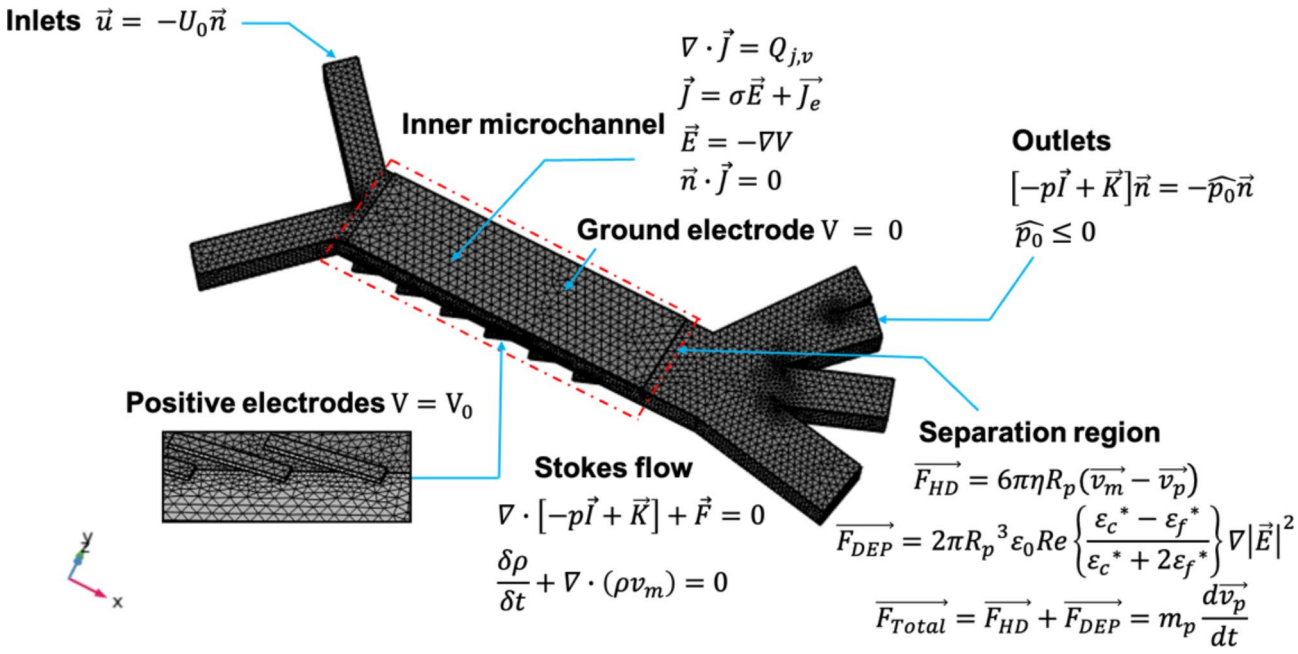

Fig. 5. Meshing model and the boundary conditions of the FEC-DEP-based device.

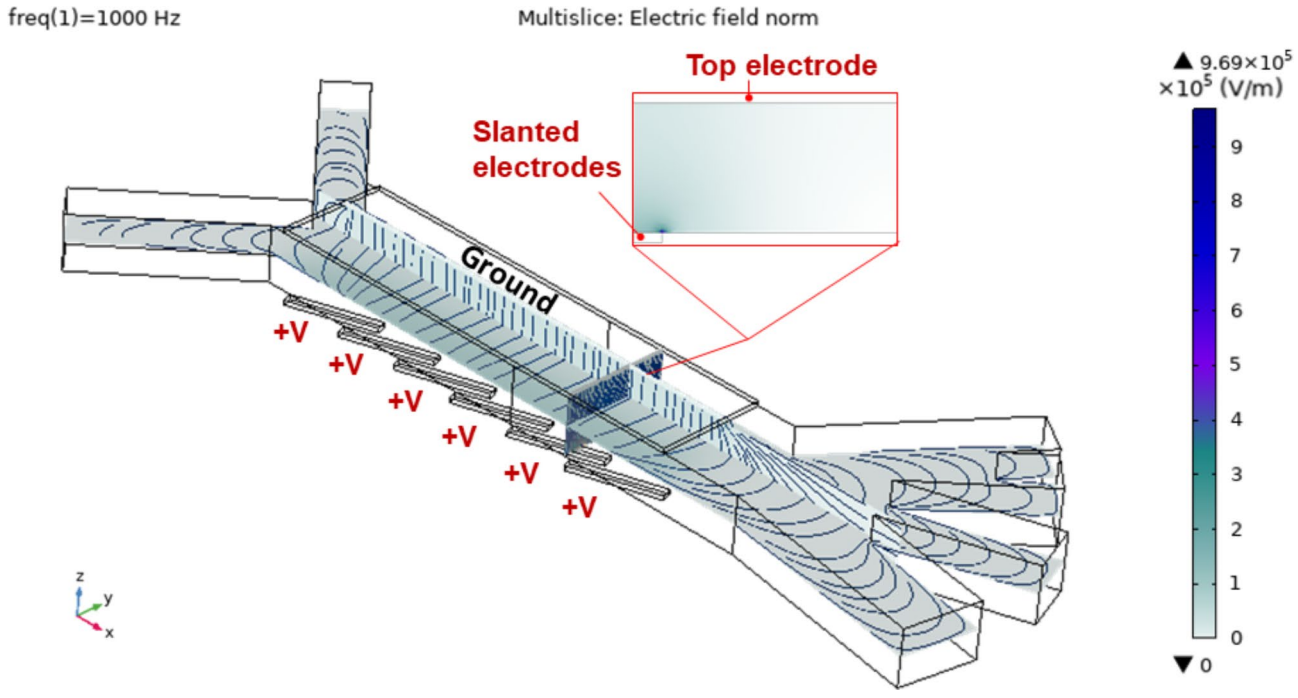

Fig. 6. Distribution of the electric field norm within the microchannel.

Results and discussion

In this section, the electric field, velocity distribution, and cell movements inside the microfluidic chip are reported. The results also indicated the influences of both operating and geometrical factors on cell trajectories including driving voltage, velocity ratio, electrode angle, channel height and the number of electrodes. While investigating the impacts of each factor, other parameters remain constant.

Separation process

Figure 6 depicts the electric field norm distribution inside the microfluidic channel. It can be seen that the regions near the positively polarized electrodes, especially at the electrode edges, feature high electric potential, resulting

in high electric field magnitude. The electric field strength decreases as the distance to the ground electrode reduces below 1×10^5 V/m. The FEC-DEP design generates a non-uniform electric field in the separation part of the microdevice, as shown in Fig. 6, which creates n-DEP effects exerting on cells and the path deflections of those cells, as seen in Fig. 7.

The Re(CM) values for CTCs and blood cells are plotted on a graph in Fig. 6, which covers the frequency range of 100 Hz to 10 GHz. The Re(CM) factor of the CTCs, RBCs, and WBCs was negative at the selected frequency of 1 kHz. The HT-29 cells, WBCs, RBCs, and PLTs exposed to varying amounts of nDEP force migrated farther away from the electrodes in both vertical and horizontal directions, or the region of low electric field gradient. Even although the Re(CM) value of WBCs was lower than that of RBCs and PLTs, the WBCs experienced the greatest deflection, indicating that the Re(CM) factor could not accurately indicate the magnitude of DEP force. According to the DEP equation, the DEP force is influenced by several factors, including the cell's electrical conductivity, permittivity, and diameter. The 1 kHz is chosen to create nDEP effects acting on all cells. In this case, the unexpected effects of electrical currents on cells are reduced since all cells moved to the top of the microchannel, which has a decreased electric field, when they entered the separation area.

The cell flow paths and electric potential cross the microchannel are illustrated in Fig. 8. The velocity steadily drops from its maximum value at the center of the channel to the lowest value at the channel side wall. The electric potential reaches its highest value at the electrode edges and decreases to zero at the ground electrode. In this simulation, a velocity ratio of 1:4.5 was maintained between the sample and buffer flows. Figure 8a shows the cell trajectories in the absence of DEP force. Simulation results show that only hydrodynamic forces from the buffer flow would force all cells toward the channel wall near the bottom electrodes. All cells migrated in the same direction from the inlet to a single outlet. As a result, the outlet would contain cells randomly arranged according to the cell distribution at the inlet. In the case of applying DEP separation, numerical computations were conducted using an excitation AC voltage of 6 V at 1 kHz. Firstly, four distinct cell types were introduced into inlet 2, while the buffer flow was pumped into inlet 1 to drive those cells towards the electrode part. Under the effects of the applied DEP force, all cell trajectories were deflected in both horizontal and vertical directions

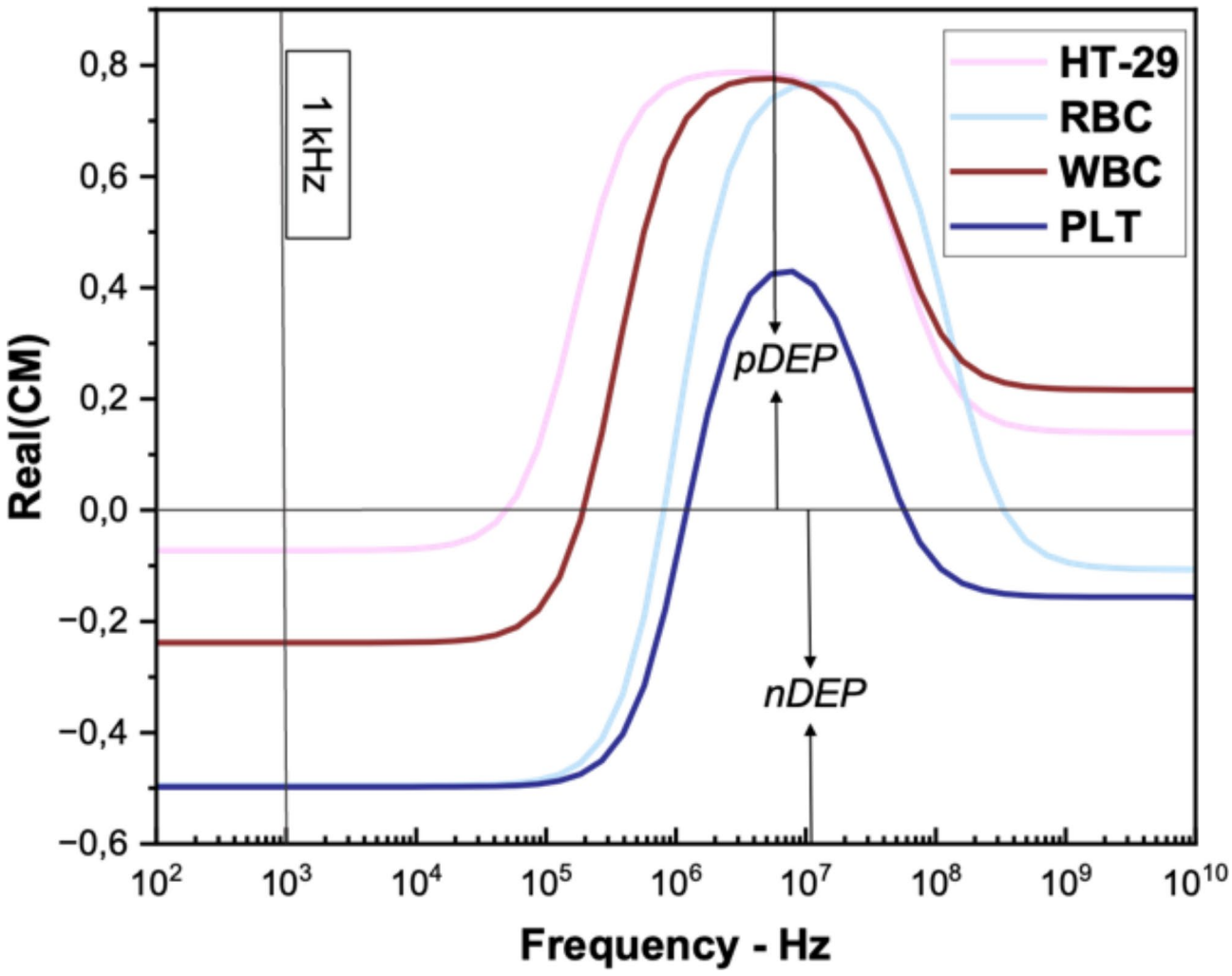

Fig. 7. The real component of the Clausius-Mossotti factor indicates that all cell types suffer nDEP at the specified frequency of 1 kHz.

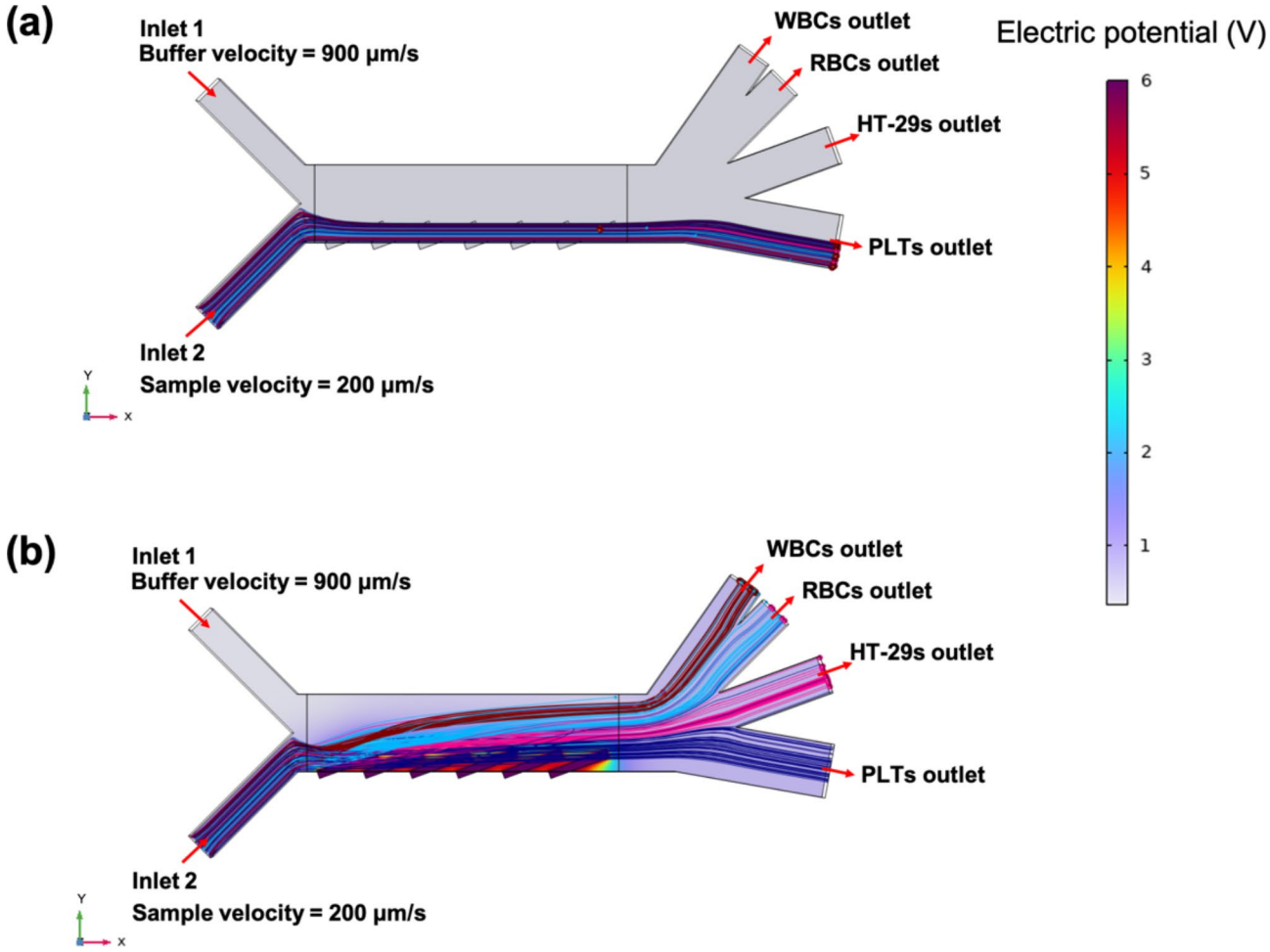

Fig. 8. Separation of CTCs from RBCs, WBCs, and PLTs in the microfluidic device without (**a**) and with (**b**) DEP force applied; electric potential within the microfluidic chip (color bar in the x-y plane).

away from the electrode region. As the WBCs, RBCs, HT-29 cells, and PLTs have their own size range and electrical properties, these cells distinctively respond to DEP effects and enrich at specified outlets (outlets 1, 2, 3, and 4 respectively).

To evaluate the FEC-DEP-based device's performance, two parameters were used: purity for each type of cell and separation efficiency. Separation efficiency, or SE, is the proportion of cells injected into the inlet that flows to the desired outflow. Separation purity, or SP, is the ratio of the number of targeted cells collected at a certain outlet to all cells collected there. The SE and SP are calculated as follows:

$$SE\,(A) = \frac{\text{Total type A cells found at the outlet of A}}{\text{Total type A cells included at the inlet}} \tag{11}$$

$$SP\,(A) \;= \frac{\text{Total type A cells found at the outlet of A}}{\text{Total all cell types found at the outlet of A}} \tag{12}$$

For HT-29 cells, RBCs, WBCs, and platelets, the SE was 80%, 74%, 100%, and 86%, respectively, at the ideal conditions in this study.

In the subsequent sections, the influence of various factors on separation efficiency and purity will be thoroughly analyzed through simulation, including the applied voltage on the electrodes, the velocity ratio between the buffer inlet and the cell inlet, the electrode tilt angle, the microchannel height, and the number of electrodes, all with the aim of optimizing the FEC-DEP microfluidic structure. Each factor affects the separation performance in different ways, and these factors can be considered sequentially to determine the optimal conditions for the proposed FEC-DEP structure, including the optimization of both flow dynamics and the electric field and its gradient within the microchannel. While flow velocity conditions primarily influence the flow dynamics within the microchannel, the remaining factors predominantly affect the electric field and its gradient. The effects of flow conditions within the channel will be presented first.

Influences of velocity ratio

The ratio between the flow rate of the buffer solution and blood sample is a major importance to control the flow field and cell trajectories. Figure 9 depicts the effect of buffer medium flow rate on the separation efficiency. To evaluate the influences of ratio of buffer velocity to cell inlet velocity, this study calculated the separation efficiency with an electric voltage frequency of 1 kHz and a constant driving voltage of 6 V. The cell velocities were fixed at 200 μm/s injected to inlet 2 while the buffer flow rate ranged from 700 μm/s to 1000 μm/s, corresponding to the ratio of 1:3.5 to 1:5. Lower buffer velocity decreases the drag force acting on particles, the DEP forces are dominant. As a result, all cells deflect towards the upper outlets. In this case, the WBC efficiency is high at 100% because WBCs concentrated at the first outlet while the other cell efficiencies are low. By contrast, higher buffer velocity increases the hydrodynamic force that particles experience, pushing all cells downward and reducing the deflection in cell trajectories. In this case, the velocity ratio was 1:5 which means the hydrodynamic force was dominant. Consequently, particles were tended to be forced to the lower outlets. The efficiency and purity of cells are low since they are collected at inappropriate outlets. When the buffer velocity was 1000 μm/s, i.e., the ratio of the blood sample speed to the buffer speed was 1:5, the SP of HT-29 cells, RBCs, WBCs, and PLTs were approximately 59%, 72%, 80%, and 98%. Successful separation of cancer cells and blood cells occurred at optimal buffer velocity of 900 μm/s or a blood sample to buffer speed ratio of 1:4.5. An HT-29 separation efficiency of 80% was attained, accompanied by a roughly 80% purity level.

Influences of the electrode tilt angle

When considering factors affecting the electrical field along the separation regions, four parameters, including electrode tilt angle, applied voltage, channel height, and electrode numbers are investigated. The electrode angle varies the repetitive electric field profile along the channel, while the channel height influences the electric field

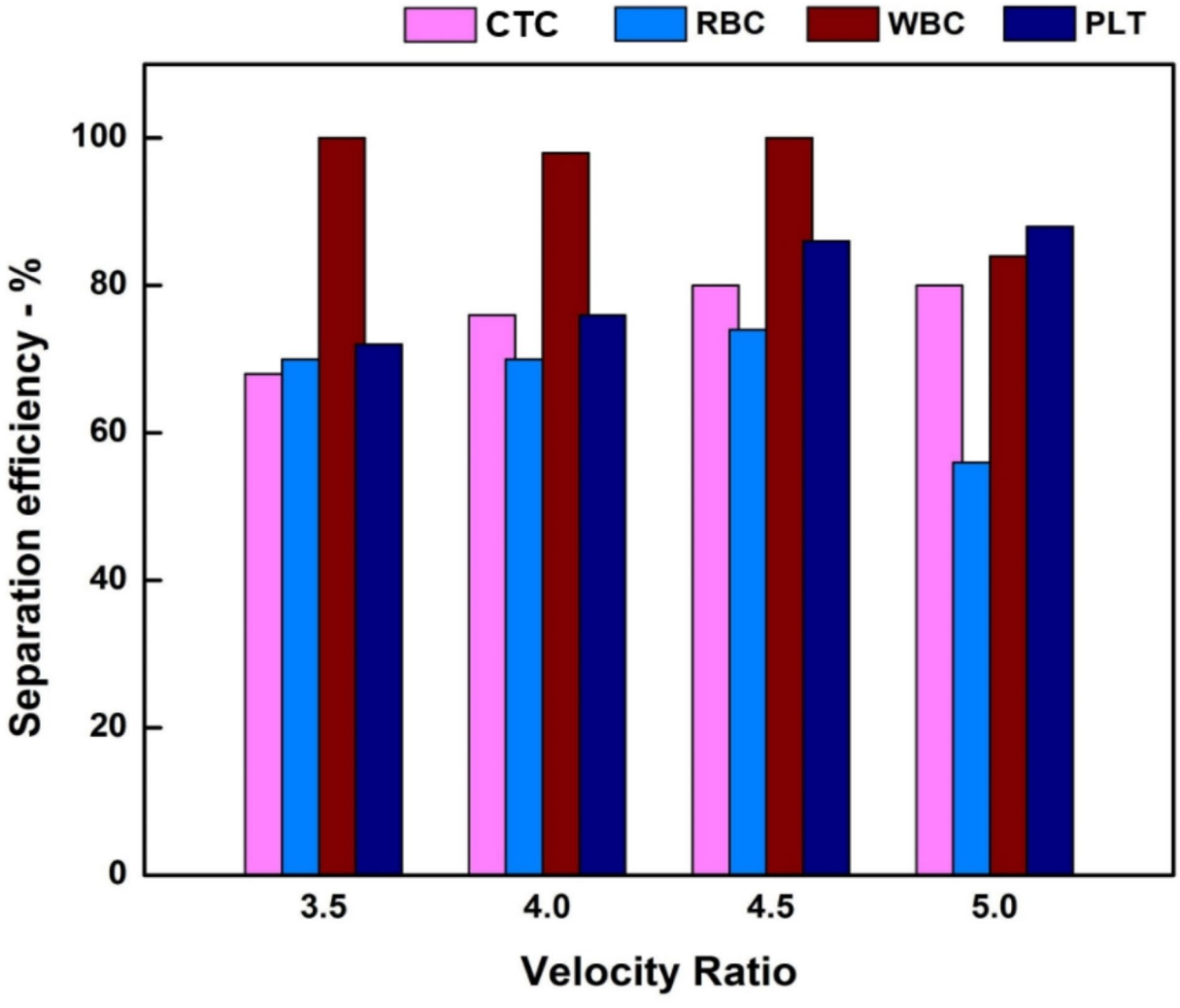

Fig. 9. Effects of the velocity ratio between the buffer inlet and the sample inlet on separation efficiency.

gradient. Meanwhile, other parameters such as applied voltage and the number of electrodes primarily scale the magnitude of the effects within this electric field profile. For these reasons, the subsequent sections will be organized as follows: the impacts of electrode tilt angle, channel height, applied voltage, and finally, the number of electrodes on the separation performance will be discussed.

The electrode tilt angle is an important geometric component with a considerable impact on the separation performance. The cell trajectories for each of the three scenarios are displayed in Fig. 10. To the y-axis, the tilted positive electrode angles were 0°, 35°, and 70°. The electric voltage frequency was always set at 1 kHz, the driving voltage was 6 V and the particle-to-buffer velocity ratio was 1:4.5. The DEP force has little effect on the trajectory of the cells moving through the channel at 0° and there was no separation. In this case, the hydrodynamic force directs all cells to the lower outlet. The electric field gradient increases with increasing electrode incidence angle, which also increases the DEP force applied horizontally to the particles. The DEP force deflected the particles in the channel with the electrodes positioned at a 35° angle, but it was insufficient to direct the particles into the appropriate outlets whereas pressure from buffer flow was dominant and forced them against the channel wall. HT-29 separation was 0% in both cases. At 70°, HT-29 purity was 80% after the most effective separation method.

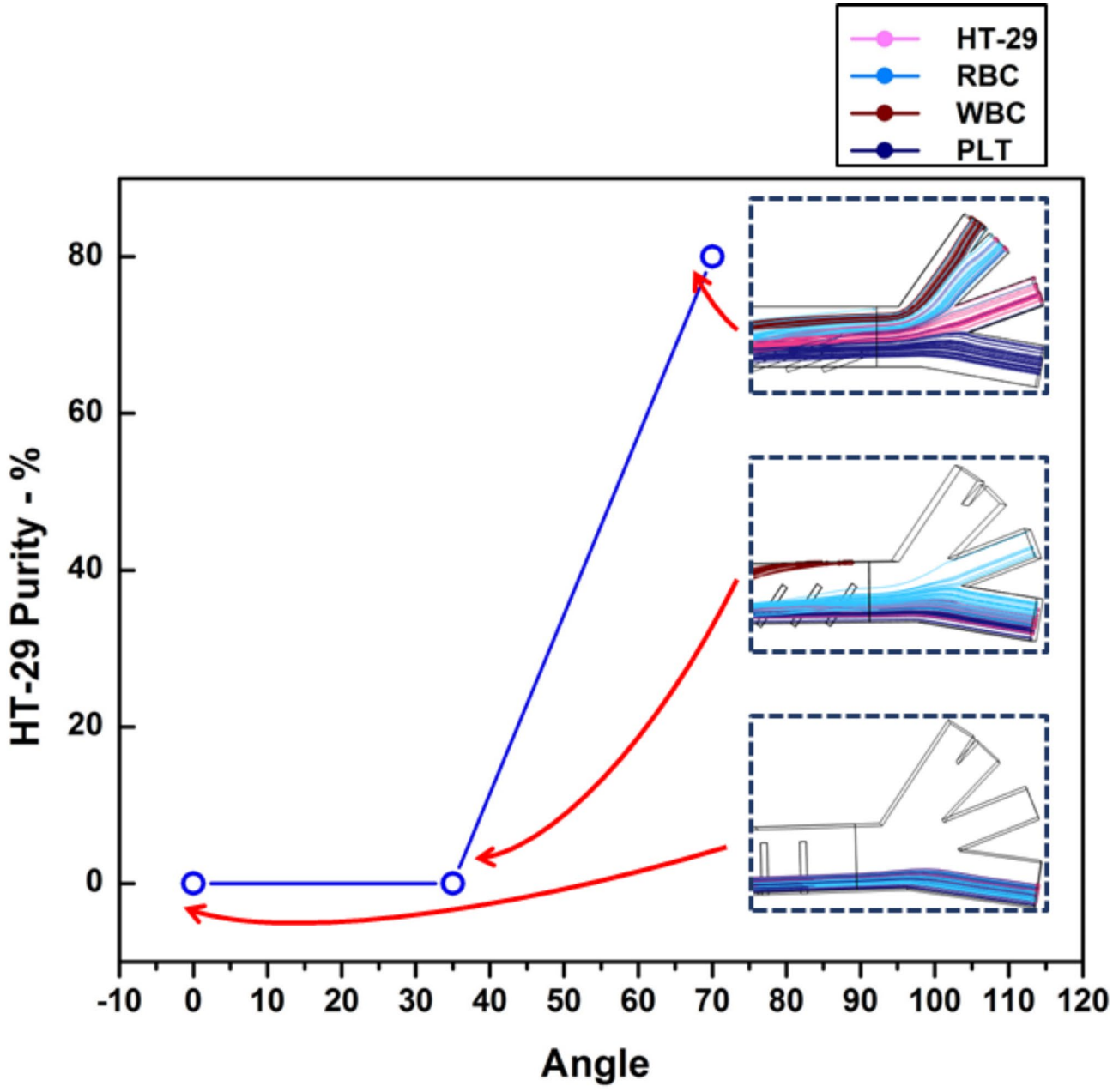

Fig. 10. Effects of the bottom electrodes' slanted angle on the purity of HT-29 purity.

Influences of microchannel height

The height of microchannel is also an important factor that contributes significantly to efficiency as the excitation electrode and the ground electrode are upper and lower structures. Because facing-electrode configuration generates non-uniform electric field all over the separation region of the microchannel, microchannel height would affect the electric field gradient. The shorter the height of the channel, the higher electric field gradient which results in greater DEP forces acting on bioparticles as the electrodes are placed closer. To evaluate the influence of microchannel height on the particle trajectories, our simulation calculated the separation efficiency with an electric voltage of 1 kHz and an applied voltage of 6 V also the velocities of cells and buffer flow ratio is 1:4,5. The channel height was assessed from 25, 50, 75 and 100 µm.

Figure 11 illustrates how lower channel height affects separation efficiency. Further electrodes distance decreases DEP force acting on particles, the drag forces were dominant. Hence, the particle tended to move toward the inner channel wall and to be collected at the downward outlets. In the 75 and 100 µm circumstances,

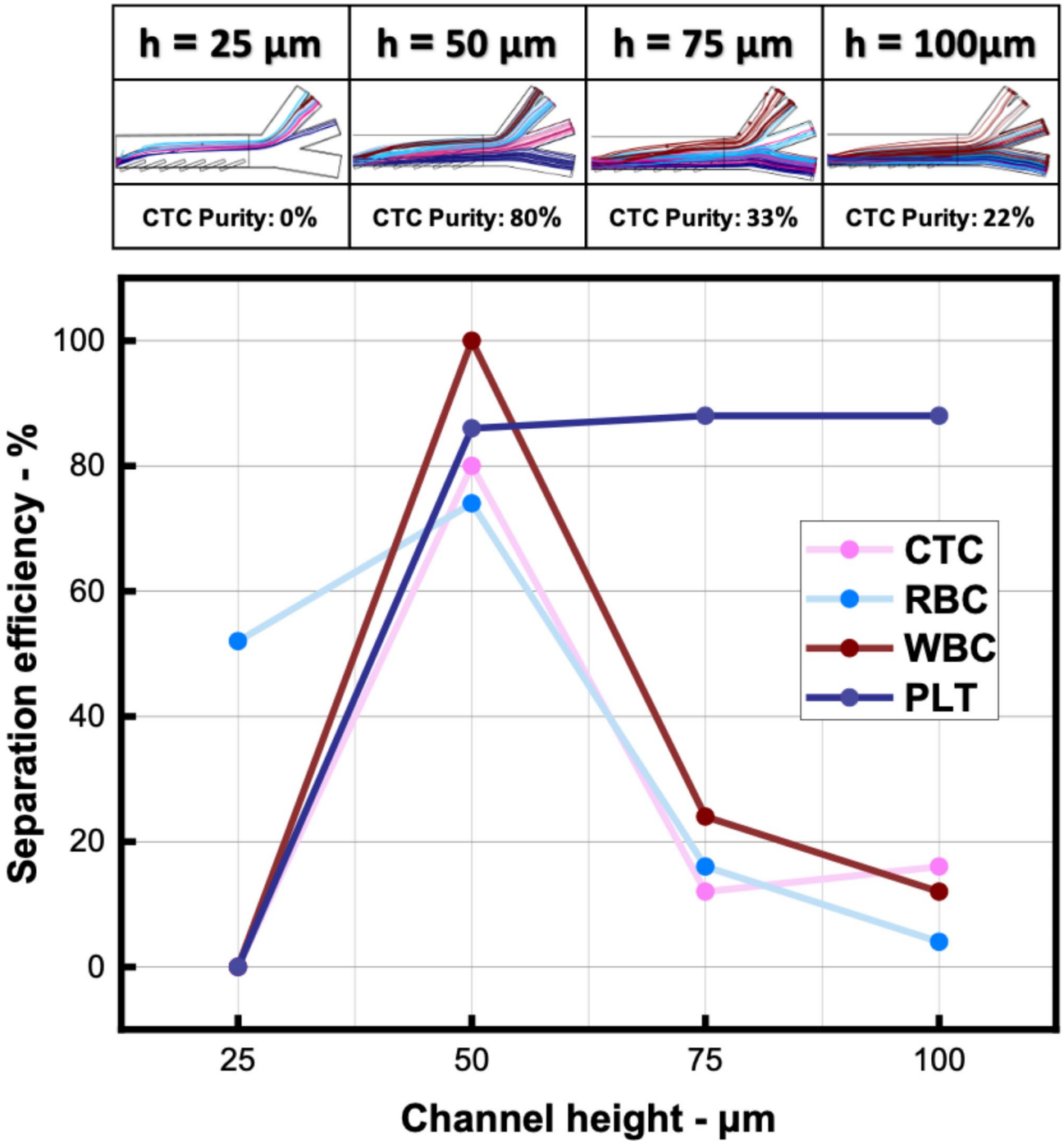

Fig. 11. Effects of the channel height on the separation efficiency.

the PLT efficiency was high because the PLTs concentrated at the lower outlet while the other cell efficiencies were low. In contrast, in the lower microchannel height case, the cells experience a higher DEP force and move toward the upward outlets. Due to the low channel, several cells, when passed through the separation region, are trapped in the upper and lower channel walls. There was no particle found at the PLT outlet and most of the particles concentrated at the RBC and CTC outlets. In our study, at 50 µm channel height the simulation results reached the highest separation efficiency and is feasible for fabrication.

Influences of applied voltage

One of the most significant aspects is the value of the driving AC voltage, which greatly affects the electric field strength and DEP forces acting on bioparticles. The separation efficiency and cell trajectories at driving voltages ranging from 5 to 7 V are shown in Fig. 12. The electric voltage frequency and cell-to-buffer ratio remained at 1 kHz and 1:4.5, respectively. According to the DEP equation, the electric field gradient increases with voltage, which should result in a greater particle deflection as voltage increases. However, the position

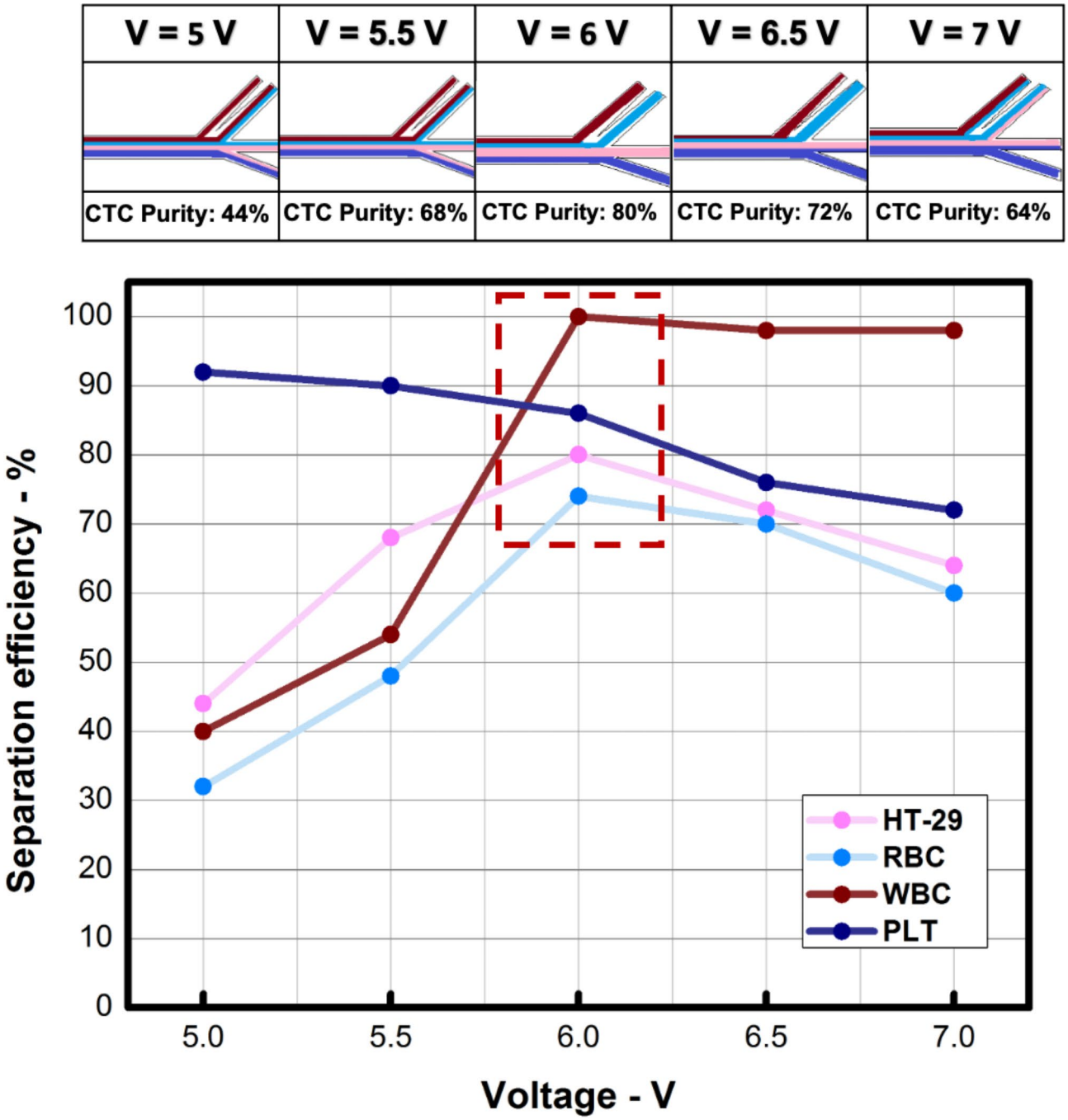

Fig. 12. Impacts of the applied voltage magnitude on separation performance.

of the outlets remains unchanged in all cases. Therefore, when cells move with a higher deflection, they tend to be collected at the upper outlets, which results in lower separation efficiency. Results show that the DEP impact increases considerably at 7 V applied voltage. In this case, particles were defected away from the positive electrode, oriented toward the WBC outflow. Around 38% of RBCs were found in the WBC outlet, and a notable number of HT-29 cells were directed toward the RBC outlet. Similarly, a portion of PLTs concentrated at the HT-29 outlet. On the other hand, at a voltage of 5 V, the DEP forces were inadequate to result in a distinguishable deflection, the HT-29 cells, WBCs, RBCs, and PLTs followed a slightly deflected path. The cell trajectories were deflected and followed the anticipated path at the ideal voltage of 6 V (Fig. 12), which produced maximum efficiency for all cell types.

Influences of the number of electrodes

Cell separation was facilitated by the non-uniform electric field generated by the FEC-DEP-based device, with the electric field's strength depending on electrode quantity and arrangement. The electric field gradient is higher as the number of electrodes increases. In this simulation, the electrode number ranged from 4 to 7, while the driving voltage was constantly set to 6 V, the electric voltage frequency was 1 kHz, and the cell velocity to buffer ratio was 1:4.5.

Figure 13 illustrates how cutting the electrode number from six to four weakens the electric field and, as a result, lowers the DEP force exerting on the cells, leading to inadequate separation and low purity levels. Using 5 electrodes, HT-29 separation efficiency was only 68% and reached 45% on the purity level.

Moreover, in the case of 4 electrodes, that figure of HT-29 was even poorer with 48% and 27% on separation efficiency and purity level, respectively. Increasing the number of electrodes from six to seven, on the other hand, increases the electric field's intensity and, therefore, the DEP force acting on the cell particles. Because the intended DEP effect was present in both situations, the separation efficiency was pretty equal. On the other hand, while employing six electrodes, the purity level of RBCs is almost 80%, which is slightly greater than when utilizing seven electrodes (roughly 76%). The reason for this is that more HT-29 cells were gathered at the RBC outflow because of their larger deflection angle.

It can be observed that the electrical field strength and the resultant lateral shift of cells change as the change of the applied voltage gradient throughout the channel, whereas the lateral shift of cells may roughly scale as the number of electrodes. Therefore, the lateral shift of cells can be varied in an analogous way by the applied voltage as well as the number of electrodes. In experimental investigations, increasing the applied voltage is preferable to modifying the number of electrodes, as it can be implemented more easily without necessitating changes to the device's design and allows for adjustments during operation.

The process of cell separation has significant importance in a broad range of life sciences applications. Besides cancer cell isolation, the separation of blood components is essential for cell analysis, disease detection, understanding of cell functions and in vivo mechanisms, and precision medicine. Recently, there have been several studies utilizing DEP to separate CTCs; however, these works mostly focused on the isolation of just two specific cell types[31,32,49–52]. Shamloo and Kamali have suggested a novel DEP-based microfluidic chip with curved outlet which successfully separated PLTs, RBCs, T-lymphocytes, and MD-231 cancer cells[53]. Nevertheless, this work used sidewall electrode configuration, which may encounter complex fabrication processes. In a previous study, a combination of DEP and magnetophoresis (MAP) in a microfluidic platform was presented and showed its capability to completely separate CTCs, RBCs, WBCs, and PLTs[15]. Although achieving high efficiency, the integration of both MAP and DEP into a device presents challenges in terms of complexity and control. Therefore, we presented in this work the FEC-DEP, which utilized a facing electrode configuration device to separate not only CTCs but also other blood components in four outlets. The obtained results have demonstrated the ability of the FEC-DEP to isolate CTCs, RBCs, WBCs, and PLTs with high efficiency and purity in a simpler configuration.

DEP-based biochips have emerged as a powerful tool for the transportation, accumulation, separation, and characterization of micro-/nano-scale bioparticles in microfluidic systems[54–56].

The application of our FEC-DEP separation techniques could be extended beyond cancer cells and blood cells, including several biological entities such as stem cells, DNA, algae, yeast, or bacteria. Therefore, this device shows significant potential for a wide range of applications in the field of biomedical and biotechnology, including cell research, oncology, stem cell studies, bacterial infection analysis, DNA research, and more. The proposed FEC-DEP structure is feasible for experimental fabrication based on established techniques. This includes the use of SU-8 patterned opposite ITO electrodes[57,58], SU-8 membranes coated on ITO[59], and PDMS with Chromium/Gold-coated glass slides[60]. These methods have been successfully applied in previous studies, demonstrating the practicality of fabricating the FEC structure.

Conclusions

This study offers an efficient FEC-DEP-based microfluidic chip designed for separating HT-29 cancer cells from RBCs, WBCs, and PLTs. The biochip design performance was confirmed and examined using numerical evaluation. By using the FEC-DEP structure, DEP force is applied to bioparticles, enabling reduced cell position dependence in the channel and simplified fabrication complexity. The effects of the geometric and operational features were examined; under optimal conditions, there was a high separation efficiency and purity for WBCs, RBCs, PLTs, and HT-29. The HT-29 tumor cells were effectively collected at the designated outlet. Results showed how the geometric and physical characteristics of the proposed device influence particle trajectories and separation efficiency. This study laid a strong foundation for further experimental research by proposing and validating the feasibility of the FEC-DEP platform through numerical analysis, with planned experiments set to further assess and refine the device's performance. The FEC-DEP-based system has many benefits, such as being label-free, non-invasive, small in size, low applied voltage, and very efficient. The biochip has the potential

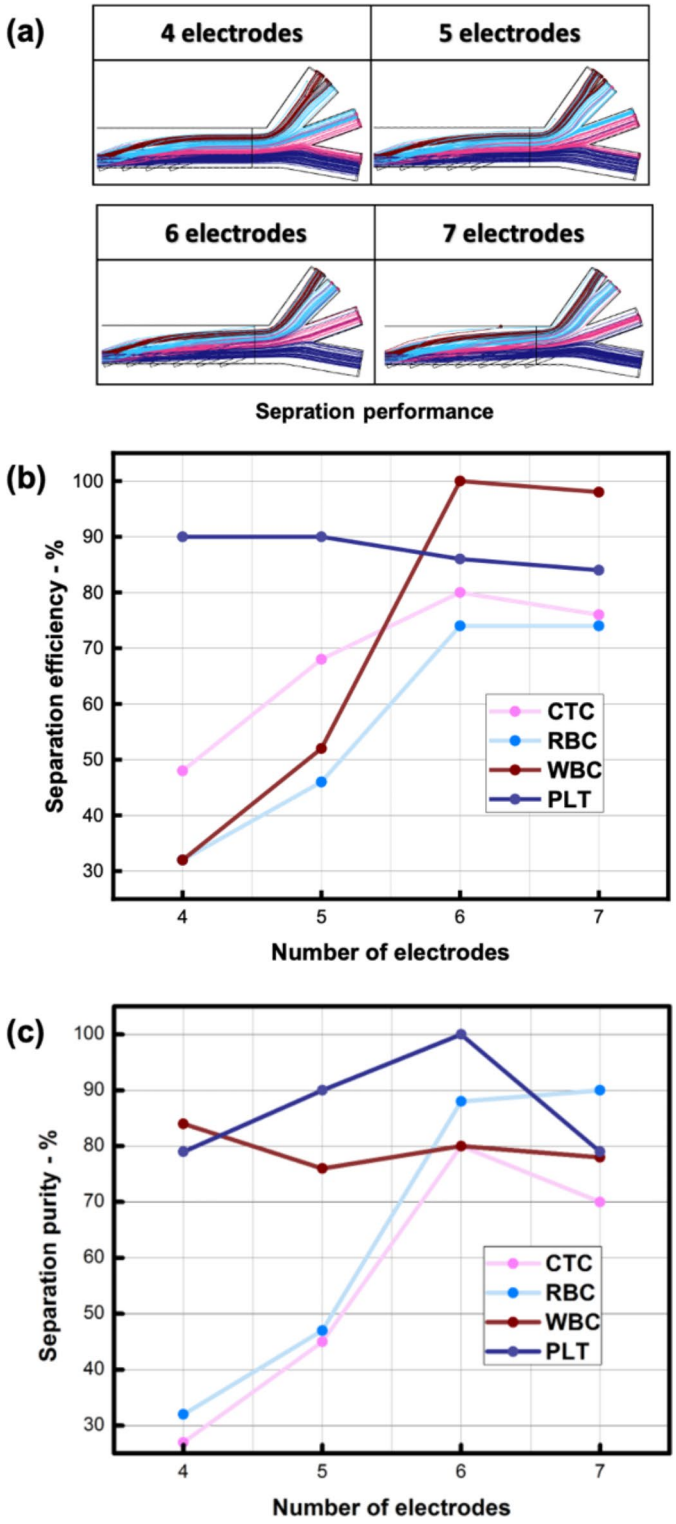

Fig. 13. Impacts of the number of bottom electrodes on separation performance (**a**), separation efficiency (**b**), and separation purity (**c**).

to be used for the manipulation, detection, assessment, and analysis of cancer and could also be used on diverse biological objects, including stem cells, reproductive cells, dead and viable cells, etc.

Data availability

All data generated or analysed during this study are included in this article or from the corresponding authors upon reasonable request.

Received: 23 June 2024; Accepted: 4 November 2024
Published online: 11 November 2024

References

1. Spell, D. W., Jones, D. V., Harper, W. F. & Bessman, J. D. The value of a complete blood count in predicting cancer of the colon. *Cancer Detect. Prev.* **28**, 37–42 (2004).
2. Christensen, R. D., Henry, E., Jopling, J. & Wiedmeier, S. E. The CBC: Reference ranges for neonates. *Semin. Perinatol.* **33**, 3–11 (2009).
3. Lin, D. et al. Circulating tumor cells: Biology and clinical significance. *Signal Transduct. Target. Ther.* **6**, 1–24 (2021).
4. Castro-Giner, F. & Aceto, N. Tracking cancer progression: From circulating tumor cells to metastasis. *Genome Med.* **12**, 1–12 (2020).
5. Eslami-S, Z., Cortés-Hernández, L. E., Thomas, F., Pantel, K. & Alix-Panabières, C. Functional analysis of circulating tumour cells: The KEY to understand the biology of the metastatic cascade. *Br. J. Cancer* **127**, 800–810 (2022).
6. Jackson, E. L. & Lu, H. Advances in microfluidic cell separation and manipulation. *Curr. Opin. Chem. Eng.* **2**, 398–404 (2013).
7. Aghlmandi, A. et al. Microfluidics as efficient technology for the isolation and characterization of stem cells. *EXCLI J.* **20**, 426 (2021).
8. Jahangiri, A. R. et al. Microfluidics: The future of sperm selection in assisted reproduction. *Andrology* **12**, 1236–1252 (2024).
9. Wu, Y. G. et al. Selection of oocytes for in vitro maturation by brilliant cresyl blue staining: a study using the mouse model. *Cell Res.* **17**, 722–731 (2007).
10. Sabbatinelli, G. et al. Isolation and enrichment of circulating fetal cells for NIPD: An overview. *Diagnostics* **11**, 2239 (2021).
11. Wyatt Shields Iv, C., Reyes, C. D. & López, G. P. Microfluidic cell sorting: A review of the advances in the separation of cells from debulking to rare cell isolation. *Lab Chip* **15**, 1230–1249 (2015).
12. Samuel, R. et al. Microfluidic—based sperm sorting & analysis for treatment of male infertility. *Transl. Androl. Urol.* **7**, S336 (2018).
13. Iwasaki, W. et al. Simple separation of good quality bovine oocytes using a microfluidic device. *Sci. Rep.* **8**, 1–9 (2018).
14. Farahinia, A., Zhang, W. J. & Badea, I. Novel microfluidic approaches to circulating tumor cell separation and sorting of blood cells: A review. *J. Sci. Adv. Mater. Dev.* **6**, 303–320 (2021).
15. Van Tran Thi, Y. et al. Design and numerical study on a microfluidic system for circulating tumor cells separation from whole blood using magnetophoresis and dielectrophoresis techniques. *Biochem. Eng. J.* **186**, 108551 (2022).
16. Sonnenberg, A. et al. Dielectrophoretic isolation and detection of cancer-related circulating cell-free DNA biomarkers from blood and plasma. *Electrophoresis* **35**, 1828–1836 (2014).
17. Luo, L. & He, Y. Magnetically driven microfluidics for isolation of circulating tumor cells. *Cancer Med.* **9**, 4207–4231 (2020).
18. Ding, X. et al. Cell separation using tilted-angle standing surface acoustic waves. *Proc. Natl. Acad. Sci. U. S. A.* **111**, 12992–12997 (2014).
19. Aguirre, G. R., Efremov, V., Kitsara, M. & Ducrée, J. Integrated micromixer for incubation and separation of cancer cells on a centrifugal platform using inertial and dean forces. *Microfluid. Nanofluidics* **18**, 513–526 (2015).
20. Glynn, M., Nwankire, C., Lemass, K., Kinahan, D. J. & Ducrée, J. Cluster size distribution of cancer cells in blood using stopped-flow centrifugation along scale-matched gaps of a radially inclined rail. *Microsyst. Nanoeng.* **1**, 1–9 (2015).
21. Shamloo, A., Naghdloo, A. & Besanjideh, M. Cancer cell enrichment on a centrifugal microfluidic platform using hydrodynamic and magnetophoretic techniques. *Sci. Rep.* **11**, 1–14 (2021).
22. Li, Y. et al. On the design, functions, and biomedical applications of high-throughput dielectrophoretic micro-/nanoplatforms: A review. *Nanoscale* **13**, 4330–4358 (2021).
23. Mohd Maidin, N. N., Buyong, M. R., Rahim, R. A. & Mohamed, M. A. Dielectrophoresis applications in biomedical field and future perspectives in biomedical technology. *Electrophoresis* **42**, 2033–2059 (2021).
24. Khoshmanesh, K., Nahavandi, S., Baratchi, S., Mitchell, A. & Kalantar-zadeh, K. Dielectrophoretic platforms for bio-microfluidic systems. *Biosens. Bioelectron.* **26**, 1800–1814 (2011).
25. Li, M., Li, W. H., Zhang, J., Alici, G. & Wen, W. A review of microfabrication techniques and dielectrophoretic microdevices for particle manipulation and separation. *J. Phys. D. Appl. Phys.* **47**, 063001 (2014).
26. Turcan, I. & Olariu, M. A. Dielectrophoretic manipulation of cancer cells and their electrical characterization. *ACS Comb. Sci.* **22**, 554–578 (2020).
27. Adams, T. N. G., Jiang, A. Y. L., Vyas, P. D. & Flanagan, L. A. Separation of neural stem cells by whole cell membrane capacitance using dielectrophoresis. *Methods* **133**, 91–103 (2018).
28. Karcz, A. et al. Electrically-driven handling of gametes and embryos: Taking a step towards the future of ARTs. *Lab Chip* **22**, 1852 (2022).
29. Markx, G. H., Talary, M. S. & Pethig, R. Separation of viable and non-viable yeast using dielectrophoresis. *J. Biotechnol.* **32**, 29–37 (1994).
30. Hong, B. & Zu, Y. Detecting circulating tumor cells: Current challenges and new trends. *Theranostics* **3**, 445–6362 (2013).
31. Varmazyari, V., Habibiyan, H., Ghafoorifard, H., Ebrahimi, M. & Ghafouri-Fard, S. A dielectrophoresis-based microfluidic system having double-sided optimized 3D electrodes for label-free cancer cell separation with preserving cell viability. *Sci. Rep.* **12**, 12100 (2022).
32. Nguyen, N. V., Le Manh, T., Nguyen, T. S., Le, V. T. & Van Hieu, N. Applied electric field analysis and numerical investigations of the continuous cell separation in a dielectrophoresis-based microfluidic channel. *J. Sci. Adv. Mater. Dev.* **6**, 11–18 (2021).
33. Wu, Y., Ren, Y., Tao, Y., Hou, L. & Jiang, H. High-throughput separation, trapping, and manipulation of single cells and particles by combined dielectrophoresis at a bipolar electrode array. *Anal. Chem.* **90**, 11461–11469 (2018).
34. Guan, Y. et al. Dielectrophoresis separation of platelets using a novel zigzag microchannel. *Micromachines* **11**, 890 (2020).
35. Piacentini, N., Mernier, G., Tornay, R. & Renaud, P. Separation of platelets from other blood cells in continuous-flow by dielectrophoresis field-flow-fractionation. *Biomicrofluidics* **5**, 34122–341228 (2011).
36. Liao, S. H., Chang, C. Y. & Chang, H. C. A capillary dielectrophoretic chip for real-time blood cell separation from a drop of whole blood. *Biomicrofluidics* **7**, 024110 (2013).
37. Nguyen, T. H. et al. Numerical analysis of dielectrophoresis-based microfluidic chip with a facing-electrode design for cell separation. *J. Biosyst. Eng.* **49**, 29–40 (2024).
38. Martínez-Maqueda, D., Miralles, B. & Recio, I. HT29 cell line. *Impact Food Bioact. Heal. Vitr. Ex Vivo Model.* **2**, 113–124. https://doi.org/10.1007/978-3-319-16104-4_11 (2015).
39. Romano, A. Introduction to fluid mechanics. In *Classical Mechanics with Mathematica®* 427–457 (Birkhäuser Boston, 2012). https://doi.org/10.1007/978-0-8176-8352-8_23.
40. Pakhira, W., Kumar, R. & Ibrahimi, K. M. Design and numerical simulation of a microfluidic lab-on-a-chip utilizing positive and negative dielectrophoresis technique for separation of multiple CTCs distinctly. *Comput. Part. Mech.* **2**, 1–14. https://doi.org/10.1007/S40571-024-00760-9/METRICS (2024).
41. Rahman, N. A., Ibrahim, F. & Yafouz, B. Dielectrophoresis for biomedical sciences applications: A review. *Sensors* **17**, 449 (2017).
42. Wang, X., Wang, X. B. & Gascoyne, P. R. C. General expressions for dielectrophoretic force and electrorotational torque derived using the Maxwell stress tensor method. *J. Electrostat.* **39**, 2 (1997).

43. Henriksson, A., Neubauer, P. & Birkholz, M. Dielectrophoresis: An approach to increase sensitivity, reduce response time and to suppress nonspecific binding in biosensors?. *Biosensors* **12**, 2 (2022).
44. Huang, Y., Holzel, R., Pethig, R. & Wang, X.-B. Differences in the AC electrodynamics of viable and non-viable yeast cells determined through combined dielectrophoresis and electrorotation studies. *Phys. Med. Biol.* **37**, 1499 (1992).
45. Shamloo, A., Yazdani, A. & Saghafifar, F. Investigation of a two-step device implementing magnetophoresis and dielectrophoresis for separation of circulating tumor cells from blood cells. *Eng. Life Sci.* **20**, 296–304 (2020).
46. Low, W. S. & Kadri, N. A. Computational analysis of enhanced circulating tumour cell (CTC) separation in a microfluidic system with an integrated dielectrophoretic-magnetophorectic (DEP-MAP) technique. *Chemosens.* **4**, 14 (2016).
47. Wu, L., Lanry Yung, L. Y. & Lim, K. M. Dielectrophoretic capture voltage spectrum for measurement of dielectric properties and separation of cancer cells. *Biomicrofluidics* **6**, 2 (2012).
48. Chen, J. et al. Electrodeformation for single cell mechanical characterization. *J. Micromech. Microeng.* **21**, 054012 (2011).
49. Zhang, X., Xu, X., Ren, Y., Yan, Y. & Wu, A. Numerical simulation of circulating tumor cell separation in a dielectrophoresis based Y-Y shaped microfluidic device. *Sep. Purif. Technol.* **255**, 117343 (2021).
50. Valijam, S., Salehi, A. & Andersson, M. Design of a low-voltage dielectrophoresis lab-on-the chip to separate tumor and blood cells. *Microfluid. Nanofluid.* **27**, 1–11 (2023).
51. Bakhshi, M. S., Rizwan, M., Khan, G. J., Duan, H. & Zhai, K. Design of a novel integrated microfluidic chip for continuous separation of circulating tumor cells from peripheral blood cells. *Sci. Rep.* **12**, 17016 (2022).
52. Zhang, Y. & Chen, X. Dielectrophoretic microfluidic device for separation of red blood cells and platelets: A model-based study. *J. Brazilian Soc. Mech. Sci. Eng.* **42**, 89 (2020).
53. Shamloo, A. & Kamali, A. Numerical analysis of a dielectrophoresis field-flow fractionation device for the separation of multiple cell types. *J. Sep. Sci.* **40**, 4067–4075 (2017).
54. Viefhues, M. & Eichhorn, R. DNA dielectrophoresis: Theory and applications a review. *Electrophoresis* **38**, 1483–1506 (2017).
55. Pethig, R. Dielectrophoresis: An assessment of its potential to aid the research and practice of drug discovery and delivery. *Adv. Drug Deliv. Rev.* **65**, 1589–1599 (2013).
56. Jubery, T. Z., Srivastava, S. K. & Dutta, P. Dielectrophoretic separation of bioparticles in microdevices: A review. *Electrophoresis* **35**, 691–713 (2014).
57. Huang, C. . Te., Weng, C. H. & Jen, C. P. Three-dimensional cellular focusing utilizing a combination of insulator-based and metallic dielectrophoresis. *Biomicrofluidics* **5**, 2 (2011).
58. Jen, C. P., Weng, C. H. & Huang, C. T. Three-dimensional focusing of particles using negative dielectrophoretic force in a microfluidic chip with insulating microstructures and dual planar microelectrodes. *Electrophoresis* **32**, 2428–2435 (2011).
59. Chuang, Y. C., Lan, K. C., Hsieh, K. M., Jang, L. S. & Chen, M. K. Detection of glycated hemoglobin (HbA1c) based on impedance measurement with parallel electrodes integrated into a microfluidic device. *Sens. Actuators B Chem.* **171–172**, 1222–1230 (2012).
60. Cho, Y. K. et al. Bacteria concentration using a membrane type insulator-based dielectrophoresis in a plastic chip. *Electrophoresis* **30**, 3153–3159 (2009).

Acknowledgements
This work was funded by Vingroup Joint Stock Company and supported by Vingroup Innovation Foundation (VINIF) under project code VINIF.2022.DA00030. Thu Hang Nguyen was funded by the Master, PhD Scholarship Programme of Vingroup Innovation Foundation (VINIF), code VINIF.2023.TS.031.

Author contributions
Thu Hang Nguyen and Nam Anh Ngo carried out the literature review. Thu Hang Nguyen, Hoang Trung Nguyen, Mai Chi Nguyen, and Hang Bui Thu ran the simulations and analyzed the data. Thu Hang Nguyen and Loc Do Quang presented the data and wrote the manuscript. Jens Ducrée and Tung Thanh Bui reviewed and edited the manuscript. Trinh Chu Duc and Loc Do Quang reviewed, edited the manuscript, and supervised the project.

Declarations

Competing interests
The authors declare no competing interests.

Ethical approval
Not applicable.

Consent for publication
All authors have given consent to this publication.

Consent to participate
Not applicable.

Additional information

Correspondence and requests for materials should be addressed to L.D.Q.